Chemosphere 303 (2022) 134854

Contents lists available at ScienceDirect

Chemosphere

journal homepage: www.elsevier.com/locate/chemosphere

Unexpected catalytic influence of atmospheric pollutants on the formation of environmentally persistent free radicals

Li Wang [a], Danli Liang [a], Jiarong Liu [a,b], Lin Du [c], Eric Vejerano [d], Xiuhui Zhang [a,*]

[a] Key Laboratory of Cluster Science, Ministry of Education of China, School of Chemistry and Chemical Engineering, Beijing Institute of Technology, Beijing, 100081, China
[b] Key Laboratory of National Land Space Planning and Disaster Emergency Management of Inner Mongolia, School of Resources, Environment and Architectural Engineering, Chifeng University, Chifeng, 024000, China
[c] Environment Research Institute, Shandong University, Qingdao, 266237, China
[d] Center for Environmental Nanoscience and Risk, Department of Environmental Health Sciences, University of South Carolina, Columbia, SC, 29208, United States

HIGHLIGHTS

- Both acidic and basic pollutants enhance the formation of EPFRs barrierlessly.
- Pollutants act as hydrogen atom transfer catalysts for EPFRs formation.
- Acidic and basic pollutants promote EPFRs formation with different processes.
- The new insights are helpful to clarify the abundant EPFRs in polluted regions.

GRAPHICAL ABSTRACT

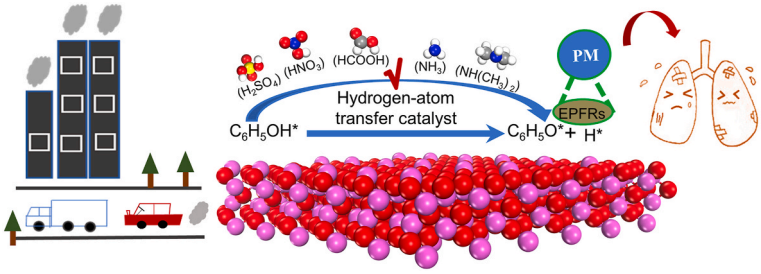

ARTICLE INFO

Handling Editor: R Ebinghaus

Keywords:
Environmentally persistent free radicals (EPFRs)
α-Al_2O_3(0001)
Acidic pollutants
Basic pollutants
Hydrogen atom transfer

ABSTRACT

Environmentally persistent free radicals (EPFRs) have been recognized as harmful and persistent environmental pollutants. In polluted regions, many acidic and basic atmospheric pollutants, which are present at high concentrations, may influence the extent of the formation of EPFRs. In the present paper, density functional theory (DFT) and ab-initio molecular dynamics (AIMD) calculations were performed to investigate the formation mechanisms of EPFRs with the influence of the acidic pollutants sulfuric acid (SA), nitric acid (NA), organic acid (OA), and the basic pollutants, ammonia (A), dimethylamine (DMA) on α-Al_2O_3 (0001) surface. Results indicate that both acidic and basic pollutants can enhance the formation of EPFRs by acting as "bridge" or "semi-bridge" roles by proceeding via a barrierless process. Acidic pollutants enhance the formation of EPFRs by first transferring its hydrogen atom to the α-Al_2O_3 surface and subsequently reacting with phenol to form an EPFR. In contrast, basic pollutants enhance the formation of EPFRs by first abstracting a hydrogen atom from phenol to form a phenoxy EPFR and eventually interacting with the α-Al_2O_3 surface. These new mechanistic insights will inform in understanding the abundant EPFRs in polluted regions with high mass concentrations of acidic and basic pollutants.

* Corresponding author.
E-mail address: zhangxiuhui@bit.edu.cn (X. Zhang).

https://doi.org/10.1016/j.chemosphere.2022.134854
Received 1 March 2022; Received in revised form 26 April 2022; Accepted 3 May 2022
Available online 6 May 2022

1. Introduction

Many countries have experienced severe atmospheric pollution due to rapid industrialization (Zhang et al., 2015). Although some policies aimed at reducing air pollution have been implemented in recent years (Jia et al., 2021), regional pollution, which is characterized by high levels of fine particulate matter (PM), still occurs frequently (Zhang et al., 2020a). It was reported that the annual average concentration of PM may exceed 65 μg m^{-3}, which adversely impacts human health, during heavy pollution conditions in Beijing (Zhao et al., 2021a). In addition to metals, inorganic, and molecular organic components, relatively newly identified pollutants, environmentally persistent free radicals (EPFRs) (Dellinger et al., 2007), also exist in significant mass concentration in PM (Chen et al., 2019; Sun et al., 2019; Wang et al., 2019, 2020a). Based on the g-factor, which is derived from electron paramagnetic resonance (EPR) measurement (Guo and Richmond-Bryant, 2021), EPFRs are generally divided into three types: semiquinone, phenoxy, and cyclopentadienyl radicals (Xu et al., 2019). Of these EPFR types, a huge amount of phenoxy-type EPFRs produced by phenolic precursors have been found abundant in haze events (Pan et al., 2019b).

Similar to the short-lived free radicals, such as hydroxyl and superoxide radicals, EPFRs can induce oxidative stress to produce immunological and inflammatory responses in cells (Zhang et al., 2020b). Thus, exposure to EPFRs is considered to be a potential threat of cardiovascular and respiratory dysfunction on human health (Balakrishna et al., 2009; Saravia et al., 2013; Gehling et al., 2014). However, unlike short-lived free radicals, EPFRs are relatively stable (i.e., they do not decompose after they are formed) and persistent (i.e., they exist for a longer period in the environment, thus transported over long distances) (Vejerano et al., 2012a; Feng et al., 2022). Accordingly, the toxic effects of EPFRs are significantly higher than traditional short-lived free radicals on human health as they are capable of redox cycling (Khachatryan et al., 2011). Thus, understanding the nature, fate, transport, and formation mechanism of EPFRs has attracted increasing research attention in recent years.

A large number of studies showed that a common pathway by which EPFRs are generated is through the interaction of aromatic compounds (e.g., phenol (Patterson et al., 2013), catechol (Qin et al., 2021), and monochlorobenzene (Truong et al., 2010) et al.) with metal oxides (such as CuO (Kiruri et al., 2014), Fe_2O_3 (Li et al., 2014), NiO (Vejerano et al., 2012b), TiO_2 (Zhao et al., 2021b), PbO (Wu et al., 2020), Al_2O_3 (Patterson et al., 2013; Cheng et al., 2022) et al.). The prevailing conceptual mechanism on the formation of EPFRs proceeds via three key steps: physisorption of an aromatic precursor on a metal surface, chemisorption, and electron transfer. During the formation process of a surface-bound EPFRs, the hydrogen or chlorine atoms dissociate from the aromatic precursors (Vejerano et al., 2018; Pan et al., 2019a). The influence of other contaminants in disrupting these steps is unknown. Notably, a large amount of EPFRs are generated in polluted air (Li et al., 2021), in which acidic and basic atmospheric pollutants are present at high concentrations. Recently, it has been reported that the concentrations of EPFRs are correlated with SO_4^{2-}, NO_3^-, and NH_4^+ during field sample analysis (Qian et al., 2020), indicating that these ions (common precursors of atmospheric particles), along with acidic and basic pollutants, such as sulfuric acid (SA) (Dai et al., 2017), nitric acid (NA) (Wang et al., 2020b), organic acid (OA) (Chen et al., 2021), ammonia (A) (Pan et al., 2016), and dimethylamine (DMA) (Mao et al., 2018) might affect the formation of EPFRs in the atmosphere. However, how these pollutants affect the formation of EPFRs, and their corresponding reaction mechanisms are unclear.

The purpose of this paper is to quantify the effects of different acidic and basic air pollutants on the formation of EPFRs and identify the corresponding formation mechanisms under the complex conditions occurring in a polluted atmosphere. Herein, the density functional theory (DFT) and ab-initio molecular dynamics (AIMD) calculations were performed to investigate the formation mechanisms of EPFRs with the influence of SA, NA, OA, A, and DMA. Phenol and Al_2O_3 were employed here as examples of aromatic precursor and metal oxide substrate, respectively, due to their high concentration in the atmosphere (Li et al., 2020; Lian et al., 2020).

2. Computational methods and models

All DFT calculations were performed via the Vienna ab initio Simulation Package (VASP 5.4.4) (Beck, 1993). The generalized gradient approximation (GGA) with the Perdew, Burke, and Ernzerhof (PBE) functional was adopted to describe electron-electron interaction (Perdew et al., 1996), and the projector-augmented wave (PAW) method was adopted to describe the interactions between ionic cores and valence electrons (Blöchl, 1994). The detailed settings of methods are listed in Text S1. The nudged elastic band (CI-NEB) method (Henkelman et al., 2000) was adopted to search for transition state structures, and the resulting structures were confirmed subsequently using the imaginary frequency vibrational analysis. All AIMD simulations were performed to reflect the chemical reactions based on the DFT method with a joint Gaussian and plane wave (GPW) formalism in CP2K 6.1 program package (VandeVondele et al., 2005). The detailed methods used in this study are listed in Text S2. Additionally, the electrostatic potential (ESP) (Lu and Manzetti, 2014) on the molecular surface was analyzed to predict the molecular properties and reactivity of these pollutants. The detailed descriptions of the properties of ESP are described in Text S3.

The Al-terminated (0001) surface of α-Al_2O_3 was used to model the Al_2O_3 substrate because it has been experimentally and theoretically demonstrated to be the most stable surface (Messaykeh et al., 2019). A 2 × 2 periodic slab with three Al–O–Al trilayers (9 atomic layers) was utilized in the reactions. The bottom one trilayer was fixed to the bulk positions, while the top two trilayers were allowed to relax. The supercell slab was repeated periodically with a 15 Å vacuum layer to separate adjacent plates. Fig. S1 presents the configurations of the relaxed α-Al_2O_3(0001). The outermost Al atoms display a significant inward relaxation, which is consistent with previous studies (Łodziana and Nørskov, 2001; Wallin et al., 2006). The detailed descriptions for the surface characteristic of the substrate are shown in Text S4.

In this work, the adsorption energies (E_{ads}) are calculated according to the following equation

$$E_{ads} = E_{(slab+adsorbate)} - E_{(adsorbate)} - E_{(slab)} \quad (1)$$

where $E_{(slab\ +\ adsorbate)}$ is the total energy of the adsorbate on the surface, $E_{(slab)}$ denotes the energy of the slab and $E_{(adsorbate)}$ denotes the energy of the gas-phase adsorbate, respectively. Thus, a more negative E_{ads} indicates stronger adsorption.

3. Results and discussion

3.1. Adsorption and dissociation of phenol for the formation of EPFRs

Several parallel and vertical adsorption configurations were constructed to investigate the adsorption of phenol on the α-Al_2O_3(0001). After full optimization, these adsorption configurations could be classified into three categories (i) vertical adsorption, (ii) parallel adsorption through the binding between the O atom of phenol and the Al atom, and (iii) parallel adsorption through the H atom of hydroxy toward the O atom of α-Al_2O_3(0001) (Fig. S2). The detailed E_{ads} and bonding lengths of these configurations are listed in Table S1 and the description of the adsorption configuration of phenol is shown in Text S5. Among these configurations, structure (ii), was the most stable with the E_{ads} of −38.1 kcal mol^{-1}, indicating a strong interaction between the phenol and the surface. Therefore, this initial structure was used in subsequent reaction studies.

Further insights into the interfacial bonding chemistry of phenol on

the α-Al_2O_3(0001) were obtained by analyzing the differences in charge density (Jayan and Islam, 2021) and the Bader charge (Henkelman et al., 2006), as shown in Fig. S3. There was a large cyan area around the H_1 atom on the hydroxyl of phenol, indicating a significant electron depletion of this region, whereas the yellow area between the O_1 atom and Al_1 atom suggests the higher electron density in this region. Meanwhile, another yellow area between the aromatic ring and the surface also shows significant charge redistributions at the interface. The analysis of the Bader charge shows that after the adsorption of phenol, the electrons of O_1 atom increase by 0.14 |e| and the electrons of H_1 atom decrease by 0.07 |e|, which directly corroborates with the results obtained from the charge density difference analysis. Therefore, the adsorption of phenol induces a partial polarization of phenol on the surface, in which the O_1 atom of phenol could interact with Al_1 atom more easily and the H_1 could be attracted by the atom with high electronegativity.

Generally, the dissociative adsorption of phenol by breaking the O–H bond leads to the coadsorbed phenoxy radical and a hydrogen atom (Li et al., 2015; Pan et al., 2019b; Ahmed et al., 2020). To determine the most stable configurations of dissociative adsorption of phenol, we considered several adsorption configurations of the phenoxy radicals and hydrogen atoms on the α-Al_2O_3(0001) depending on the different orientations and sites. The optimized structures of phenoxy radicals and the hydrogen atom on the α-Al_2O_3(0001) could be classified into two main categories, respectively, as shown in Figs. S4 and S5. The corresponding E_{ads} and equilibrium distances are listed in Tables S2 and S3, respectively. The detailed adsorption configurations are shown in Text S5. Results show that structure (ii) with parallel adsorption of phenoxy on the surface was the most stable. While for the adsorption of the hydrogen atom, structure (i) was the most stable with the H atom binding to the O atom of the surface. For clarity, the subscript on an atom denotes the position in the molecule, not the number of atoms.

Based on the most stable configurations, potential energy profiles were carried out to investigate the formation process of EPFRs. As shown in Fig. 1, in this process, the O_1–H_1 bond of phenol was broken and the H_1 atom of phenol was transferred to the O_{surf} atom (surf: for the surface) with an energy barrier of 8.8 kcal mol^{-1}. The reaction energy of the formation of co-adsorbed phenoxy radical and a hydrogen atom on the surface was −23.2 kcal mol^{-1}, indicating that the formation of EPFRs is thermodynamically favorable. In addition, this reaction occurred with the transfer of the hydrogen atom from the hydroxyl of phenol to the surface, indicating that the formation of EPFRs might be affected by some species that can act as relatively strong hydrogen atom donors/acceptors.

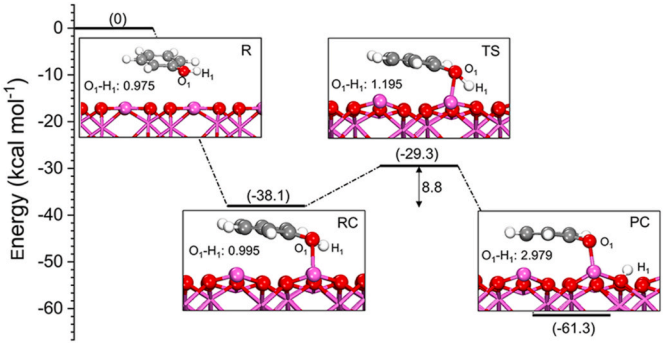

Fig. 1. The potential energy profiles for the formation of EPFRs on α-Al_2O_3(0001) with the most stable adsorption configuration of phenol. The images show the four optimized geometries of the reactant (R), reactant complex (RC), transition state (TS), and product complex (PC) for the formation of EPFRs. The bond lengths are in units of Å. Color scheme: Al, pink; O, red; C, grey; H, white. (For interpretation of the references to color in this figure legend, the reader is referred to the Web version of this article.)

3.2. The influence of pollutants on the formation of EPFRs

High concentrations of acidic and basic atmospheric pollutants are present in polluted areas. These pollutants can play important roles in the hydrogen atom transfer reactions due to their strong ability to do so (Xu et al., 2017; Liu et al., 2019). Therefore, the formation mechanism of EPFRs catalyzed by SA, NA, OA, A, and DMA on the α-Al_2O_3(0001) were further studied to clarify their contribution and impact, mimicking the conditions in polluted regions.

3.2.1. The influence of SA on the formation of EPFRs

SA is one of the most common acidic pollutants in moderately and heavily polluted areas (Yang et al., 2021). Therefore, the formation of EPFRs with the influence of SA was studied by assessing the interaction between the SA and adsorbed phenol on the α-Al_2O_3(0001) (Text S5). As shown in Fig. 2a, with SA approaching the adsorbed phenol, the H_2 and H_3 atoms of SA transferred to the surface and formed two O–H species with bond lengths of 1.054 and 1.069 Å, respectively, leaving two negatively charged O atoms. Meanwhile, the O_2 atom of SA abstracts the hydrogen atom from the broken hydroxyl group. Here, SA acts as both hydrogen atom donor and acceptor, assisting the hydrogen atom transfer from phenol to the surface. In the optimization process of co-adsorption of SA and phenol, the potential energy showed a decreasing trend from reactants to products with the increase of O_1–H_1 distances and the decrease of O_2–H_1 distances (Fig. 2b), indicating the formation of EPFRs catalyzed by SA is barrierless.

The corresponding electron localization function (ELF) was computed and analyzed (Savin et al., 1997) to identify changes in the chemical bonding character during EPFRs formation (Fig. 2c and d). ELF value ranges from 0 to 1. A high value of ELF denotes higher electron localization and vice versa (He et al., 2018). Regions of the largest and smallest localization electron density are represented here by red and blue colors, respectively. In Fig. 2c and d, the red areas adjacent to O_2–H_1, O_{surf}-H_2 as well as O_{surf}-H_3 indicate that the electrons locally concentrate to form O–H covalent bonds, on the contrary, the green areas adjacent to O_1–H_1 indicate that there are only weak interactions between them. Therefore, there is a significant electron redistribution in these regions, resulting in the transfer of the H atom of phenol to the surface via a "bridge" role of SA, in which the H atom of phenol transfers to SA and the H atoms of the SA transfer to the surface. In summary, we conclude that as a hydrogen atom transfer catalyst, SA can catalyze the formation of EPFRs significantly in the atmosphere. To our knowledge, no experimental data exists to corroborate the effect of SA as observed in our simulation. However, analysis of ambient particulate matter indicates that the abundance of EPFRs correlates with increasing SO_4^{2-} concentration (Qian et al., 2020).

3.2.2. The influence of NA on the formation of EPFRs

In addition to SA, NA is another key acidic pollutant in the atmosphere (Bouo et al., 2011). The concentrations of NA are high because it is the product of the oxidation processes of NO_x generated from many natural and anthropogenic processes (Laughner and Cohen, 2019). Similar to SA, the interaction between the NA and adsorbed phenol on the α-Al_2O_3(0001) was investigated to clarify the influence of NA on the formation of EPFRs. As shown in Fig. 3a, with NA approaching the adsorbed phenol, the distance of O_3–H_2 of NA increased to 1.769 Å, whereas the distance of O_{surf}-H_2 decreased to 0.990 Å, indicating that the hydroxyl of NA is broken and the H atom of NA is transferred to the O atom of the surface. Meanwhile, the distance of O_1–H_1 of phenol increased to 1.444 Å, whereas the distance of O_2–H_1 decreased to 1.077 Å, indicating that the hydroxyl of phenol is broken and the corresponding H atom of hydroxyl is transferred to the O_2 atom of NA. In addition, similar to the impact of SA, the potential energy decreased monotonically with the increase of O_1–H_1 distances and the decrease of O_2–H_1 distances during the formation of phenoxy, as depicted in Fig. 3b, indicating that the hydroxyl of phenol has been dissociated without an energy barrier.

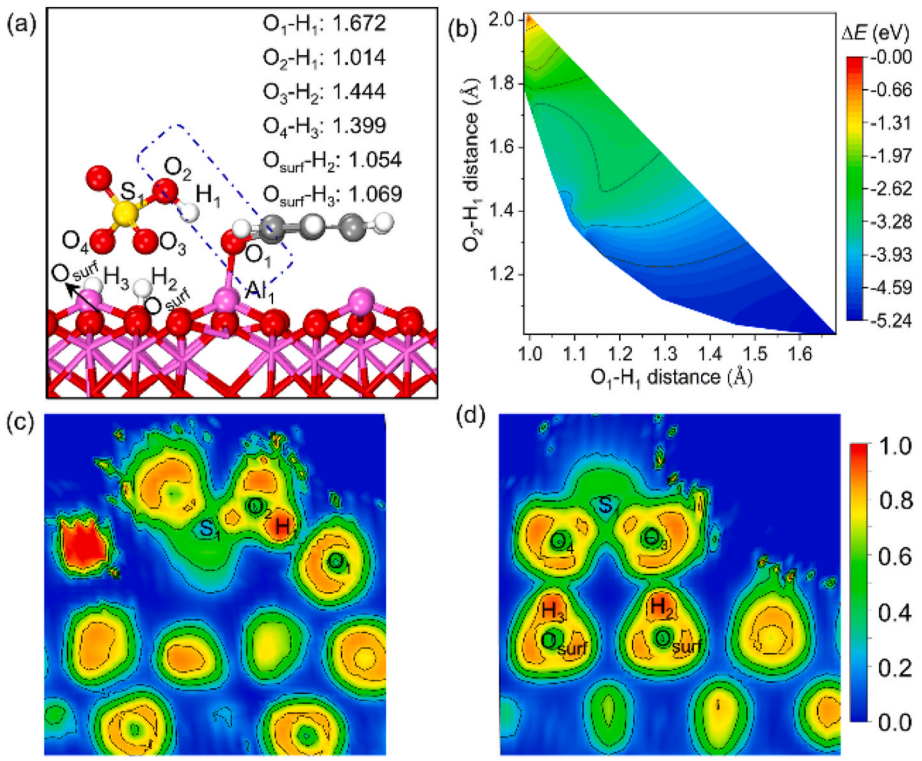

Fig. 2. (a) Geometric configuration for the participation of SA in the formation of EPFRs. (b) Change of potential energy with the varying distances of O_1–H_1 and O_2–H_1. The specific atom of O_1, H_1, and O_2 are marked with a blue rectangle shown in (a). (c) Two-dimensional electron localization function (ELF) color-filled maps in the O_1–H_1–S_1 plane. (d) ELF color-filled maps in the S_1–H_2–H_3 plane. The listed bond lengths are in units of Å. Color scheme: Al, pink; O, red; C, grey; H, white; S, yellow. (For interpretation of the references to color in this figure legend, the reader is referred to the Web version of this article.)

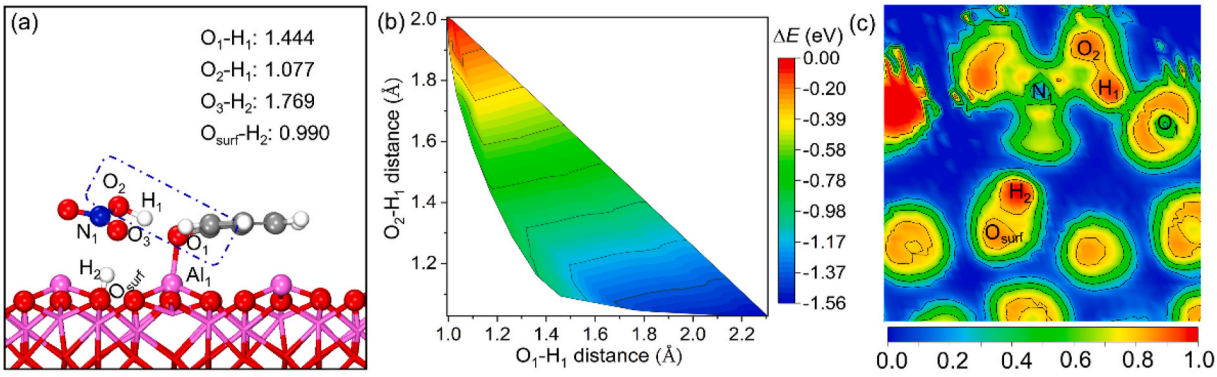

Fig. 3. (a) Geometric configuration for the participation of NA in the formation of EPFRs. (b) Change of potential energy with the distances of O_1–H_1 and O_2–H_1. The specific atom of O_1, H_1, and O_2 are marked with a blue rectangle shown in (a). (c) Two-dimensional electron localization function (ELF) color-filled maps in the O_1–N_1–H_2 plane. The listed bond lengths are in units of Å. Color scheme: Al, pink; O, red; C, grey; H, white; N, blue. (For interpretation of the references to color in this figure legend, the reader is referred to the Web version of this article.)

Based on ELF analysis (Fig. 3c), the large green regions between H_1 and O_1 as well as the red regions between H_1 and O_2 provide evidence that the transfer of H_1 atom from phenol to NA is completed. The transfer of H_2 atom from NA to the surface is also completed as indicated by the blue regions between H_2 and N_1 as well as the red regions between H_2 and O_{surf}. Overall, the H atom of phenol is transferred to the surface by which NA acts as a "bridge" via a barrierless process. These results suggest that NA in the atmosphere can significantly enhance the EPFRs formation by promoting the transfer of hydrogen atoms.

3.2.3. *The influence of OA on the formation of EPFRs*

Low molecular weight OA are common chemical components in the atmosphere (Chen et al., 2021). In our simulation, we used formic acid (FA) as a surrogate of OA because it is among the most abundant components (Tsai and Kuo, 2013) and the simplest organic acid. As shown in Fig. 4a, with the influence of FA, the hydroxyl of FA has been dissociated with an elongated O_3–H_2 distance of 1.816 Å and the H_2 atom of FA is transferred to the O_{surf} atom with a bond length of 0.922 Å. Simultaneously, the O_1–H_1 bond distance of phenol increased to 1.710 Å and the distance of the O_3–H_1 decreased to 1.023 Å, indicating that the hydroxyl of phenol is broken and the corresponding H atom of hydroxyl is transferred to the O atom of FA completely. In addition, compared with the dissociation of phenol without FA, the formation of phenoxy EPFRs catalyzed by FA is barrierless due to the monotonic decrease of the potential energy with the increase of O_1–H_1 distances and the decrease of O_3–H_1 distances (Fig. 4b).

The contour map of ELF of the O_1–O_3–H_2 plane was analyzed to investigate the effect on forming and cleaving of bonds during the process of EPFRs formation (Fig. 4c). The red areas adjacent to O_3–H_1 and O_{surf}-H_2 indicate the formation of an O–H covalent bond, whereas the areas adjacent to O_1–H_1 and O_3–H_2 indicate that the electrons are highly delocalized with weak interaction. Therefore, similar to SA and

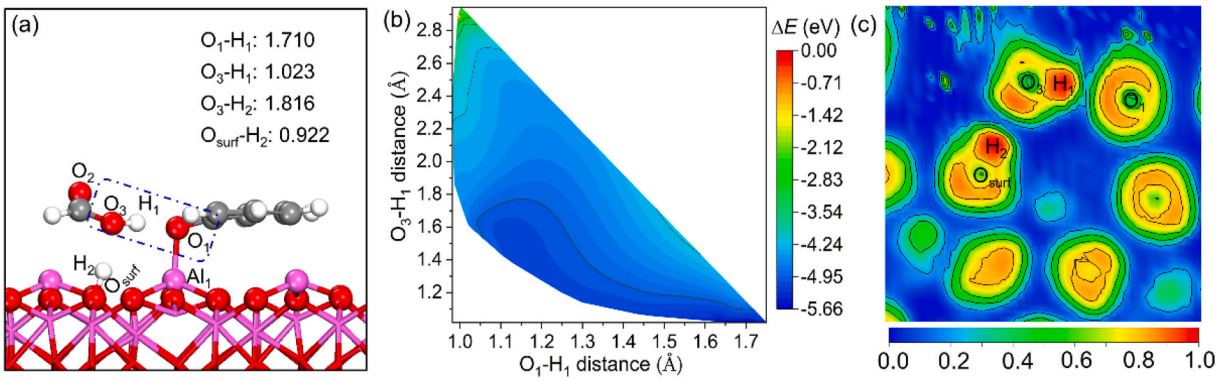

Fig. 4. (a) Geometric configuration for the participation of FA on the formation of EPFRs. (b) Change of potential energy with the varying distances of O_1–H_1 and O_3–H_1. The specific atom of O_1, H_1, and O_3 are marked with a blue rectangle shown in (a). (c) The two-dimensional electron localization function (ELF) color-filled maps in the O_1–O_3–H_2 plane. The listed bond lengths are in units of Å. Color scheme: Al, pink; O, red; C, grey; H, white. (For interpretation of the references to color in this figure legend, the reader is referred to the Web version of this article.)

NA, the H atom of phenol is transferred to the surface by a "bridge" role of FA. We speculate that other low molecular weight organic acids can also enhance the formation of EPFRs in polluted areas via the same mechanism.

3.2.4. The influence of A on the formation of EPFRs

In addition to the acidic pollutants, there are plenty of basic pollutants in polluted regions as well. Particularly, A is abundant in urban, agricultural areas, and industrialized regions (Chang et al., 2019). As shown in Fig. 5a, in the presence of A, the bond length of O_1–H_1 was 2.306 Å and the bond length of N_1–H_1 was 1.028 Å, suggesting that phenol has been dissociated and the corresponding H_1 atom formed a new bond with the N atom of A. Simultaneously, the bond lengths of N_1–H_2 and O_{surf}-H_2 were 1.525 Å and 1.074 Å, respectively, suggesting that the N_1–H_2 bond is broken and the H_2 atom of A is transferred to the O_{surf} atom. As shown in Fig. 5b, during the formation of phenoxy EPFRs, the corresponding potential energy decreased monotonically with the increase of O_1–H_1 distance and the decrease of N_1–H_1 distance, which indicates that the formation of phenoxy EPFRs with the influence of A is barrierless.

The relationship between electronic structure and geometric structure was further investigated by the analysis of ELF (Fig. 5c). In the corresponding ELF distribution map, the larger blue regions between H_1 and O_1 and the red regions between H_1 and N_1 indicate that the H_1 atom is completely transferred from phenol to A. The green regions between H_2 and N_1 and the red regions between H_2 and O_{surf} indicate that the H_2 atom is completely transferred from A to the surface. Therefore, the hydrogen atom transfer reaction catalyzed by A is similar to that catalyzed by previous acidic pollutants discussed above because of the similar distribution for local electrons. Thus, A could significantly enhance the formation of EPFRs by acting as a hydrogen atom transfer catalyst.

3.2.5. The influence of DMA on the formation of EPFRs

Amines are emitted by a wide range of sources and are ubiquitous atmospheric organic bases (Ge et al., 2011). DMA has attracted much attention in recent years due to the relatively high atmospheric concentrations (Julin et al., 2018). Therefore, it is necessary to explore the impact of DMA on EPFRs formation. As shown in Fig. 6a, in the presence of DMA, the distances of O_1–H_1 and N_1–H_1 showed that the hydroxyl of phenol was dissociated and the H atom of phenol was transferred to DMA. Furthermore, we observed that the H_2 of DMA remained bonded with the N atom with a bond length of 1.110 Å rather than formed a new bond with O_{surf}, suggesting that DMA prefers to form $DMAH^+$ rather than transfer the hydrogen atom to the surface. Thus, SA, NA, FA, and A act as a "bridge", while DMA serves as a "semi-bridge" role in EPFRs formation. In addition, as shown in Fig. 6b, the corresponding potential energy decreased monotonically with the increase of O_1–H_1 distances of phenol and the decrease of N_1–H_1 distances during the formation of phenoxy EPFRs, suggesting that the formation of EPFRs with the influence of DMA is barrierless.

ELF analysis was performed to further identify the impact of DMA on the formation mechanism of EPFRs. The red areas adjacent to N_1–H_1 and N_1–H_2 indicate that the electrons are highly localized with strong covalent bonds of N_1–H_1 and N_1–H_2. The green areas between H_2 and O_{surf} indicate that there are weak interactions between DMA and the surface.

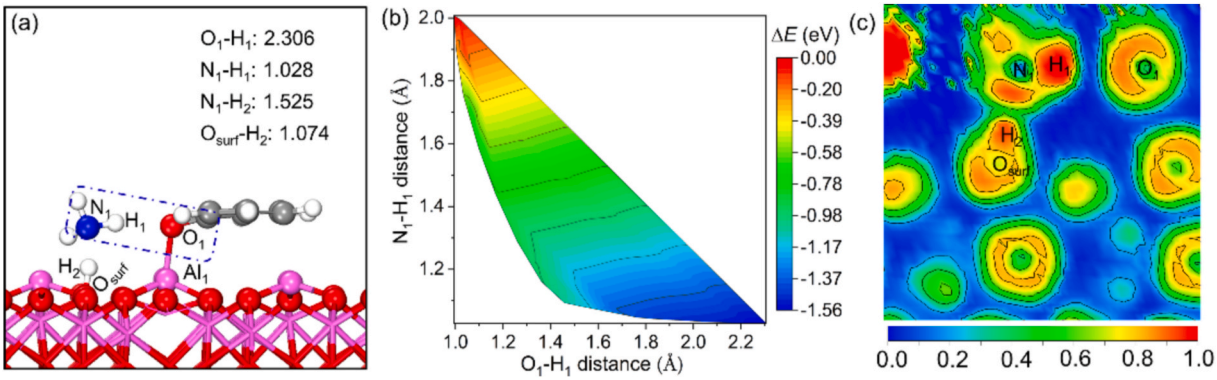

Fig. 5. (a) Geometric configuration for the participation of A in the formation of EPFRs. (b) Change of potential energy with the distances of O_1–H_1 and N_1–H_1. The specific atom of O_1, H_1, and N_1 are marked with a blue rectangle shown in (a). (c) The two-dimensional electron localization function (ELF) color-filled maps in the O_1–N_1–H_2 plane. The listed bond lengths are in units of Å. Color scheme: Al, pink; O, red; C, grey; H, white; N, blue. (For interpretation of the references to color in this figure legend, the reader is referred to the Web version of this article.)

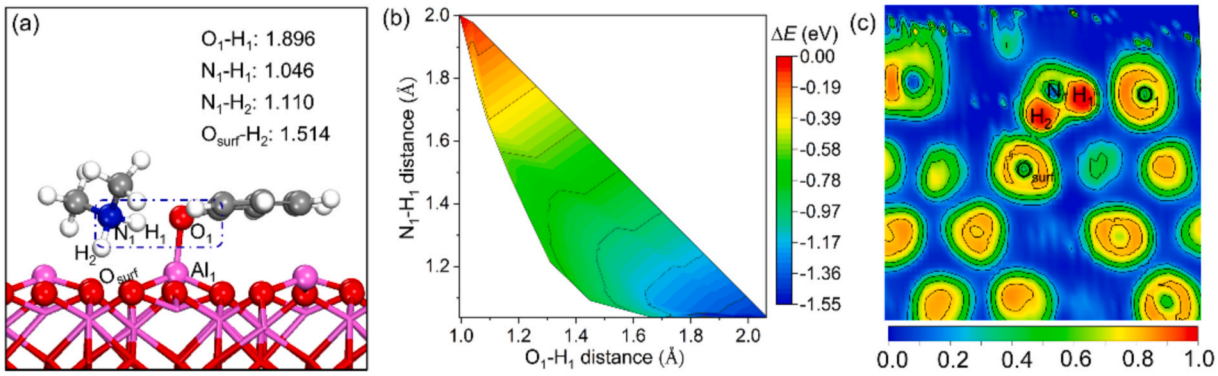

Fig. 6. (a) Geometric configuration for the participation of DMA in the formation of EPFRs. (b) Change of potential energy with the distances of O_1–H_1 and N_1–H_1. The specific atom of O_1, H_1, and N_1 are marked with a blue rectangle shown in (a). (c) The two-dimensional electron localization function (ELF) color-filled maps in the O_1–N_1–H_2 plane. The listed bond lengths are in units of Å. Color scheme: Al, pink; O, red; C, grey; H, white; N, blue. (For interpretation of the references to color in this figure legend, the reader is referred to the Web version of this article.)

The blue areas adjacent to O_1–H_1 indicate that electrons are highly delocalized with the dissociation of phenol. Therefore, the favorable formation of $DMAH^+$ promotes the dissociation of phenol (Fig. 6c). In summary, we conclude that DMA could also enhance the formation of EPFRs via a "semi-bridge" role.

In fact, besides the most stable parallel adsorption of phenol, vertical adsorption of phenol may also exist on the surface due to the relatively strong adsorption. Therefore, the influence of the above pollutants on the formation of EPFRs was also studied by considering the vertical adsorption of phenol with the binding between the O atom of phenol and the Al atom of α-Al_2O_3(0001) (structure (i)). As shown in Figs. S6-S10, the catalytic mechanism of these pollutants on the vertical adsorption of phenol is similar to that of the most stable adsorption of phenol (structure (ii)). Thus, these results confirm the promoting effect of these pollutants on EPFRs formation regardless of the orientation of phenol.

3.3. Comparison of the effect of different pollutants on the formation of EPFRs

As discussed above, SA, NA, FA, A, and DMA can all catalyze the formation of phenoxy EPFRs by promoting the dissociation of phenol, all of which are thermodynamically favorable processes (Table S4). However, after the reaction, some of the pollutants were transformed into different species depending on their properties. SA has been transformed into HSO_4^-, DMA has been transformed into $DMAH^+$, whereas NA, FA, and A retain their original molecular configurations. Therefore, it is necessary to analyze the electronic properties of each pollutant to compare their different influence on EPFRs formation.

The ESP contour plot is an important tool to illustrate the charge distributions of a molecule (Liu and Pedersen, 2009). The global maximums of ESP exhibit the strongest electrophilicity. Conversely, the global minimums exhibit the strongest electronegativity (Ning et al., 2020). As shown in Fig. S11, for the acidic pollutants, SA, NA, and FA, all possess an electron-donating region with global minimums of ESP of −26.01, −19.41, and −35.75 kcal mol^{-1}. However, they have more potential to act as donors of hydrogen atoms because the global maximums of ESP of these pollutants with +69.15, +68.18, and +62.78 kcal mol^{-1} whose absolute values are much higher than the global minimums. On the contrary, for the basic pollutants, although the global maximums of ESP have the electron-withdrawing region with the global maximums of ESP of +26.36 and + 24.39 kcal mol^{-1} respectively, they prefer to donate electrons and act as the acceptors of hydrogen atoms because the global minimums with −37.79 and −34.52 kcal mol^{-1} whose absolute values are much higher than the global maximums. Thus, the basic pollutants interacted with the hydrogen atom of phenol with the global maximums of ESP of +51.11 kcal mol^{-1}. Therefore, these pollutants with different electronic properties may have different effects on the transfer of hydrogen atoms, and the corresponding different mechanisms need to be investigated further.

Considering the electron transfer between phenol and the surface during the formation of EPFRs, the Bader charge changes of phenoxy with the impact of different pollutants were compared and shown in Fig. S12. Changes of the Bader charge of phenoxy in these reactions are negative, indicating that the phenoxy acts as the electron acceptor in all reactions. Compared with the situation of EPFRs formation without catalysts, the phenoxy obtains fewer electrons in the presence of SA, NA, and FA as catalysts. Conversely, the participation of A and DMA enhances the ability of the phenoxy to obtain more electrons. Therefore, the difference in catalytic properties of these pollutants can impact the extent of electron transfer during EPFRs formation.

As discussed above, the effects of acid and basic pollutants on the formation of EPFRs are different. Therefore, it is necessary to compare the dynamic process of EPFRs formation with the influence of acid and basic pollutants. With SA and DMA as the example of acidic and basic pollutants, respectively, AIMD simulations were performed to clarify the catalytic mechanism, as shown in Fig. 7. Under the catalysis of SA or DMA, the dissociation of phenol could occur within 1 ps, manifesting that the formation of EPFRs is barrierless in the presence of acidic and basic atmospheric pollutants. For the participation of SA (Fig. 7a and c), the H_2 atom of SA interacted with the surface initially and then transferred to the O_{surf} atom at approximately 400 fs. Subsequently, HSO_4^- interacted with the adsorbed phenol by accepting the H_1 atom of phenol. This result shows that the acidic pollutant as a hydrogen atom donor can transfer its hydrogen atom to the surface first and then combine itself with phenol to promote EPFRs formation. In contrast, as depicted in Fig. 7b and d, for the participation of DMA, initially, DMA interacted with phenol rapidly, causing the breaking of O_1–H_1 bonding of phenol and the forming of N_1–H_1 bonding at about 50 fs. Subsequently, the $DMAH^+$ interacted with the interface through a hydrogen bond. Therefore, this basic pollutant acts as a hydrogen atom acceptor by obtaining the hydrogen atom from phenol to form phenoxy EPFRs first and then interacting with the surface to promote the EPFRs formation. These results indicate that the conclusions of AIMD are consistent with that obtained from the DFT calculation.

Additionally, the AIMD simulations of the vertical adsorption of phenol with the participation of SA and DMA were performed to study the influence of these pollutants on the formation of EPFRs, which is consistent with the results discussed above (Fig. S14). Thus, we expect that in general, the impact of other acidic and basic pollutants will behave similarly to the surrogate pollutants considered in our study due to their similar chemical properties. Therefore, acidic and basic pollutants have different influences on the formation of EPFRs, which are summarized in Table S5.

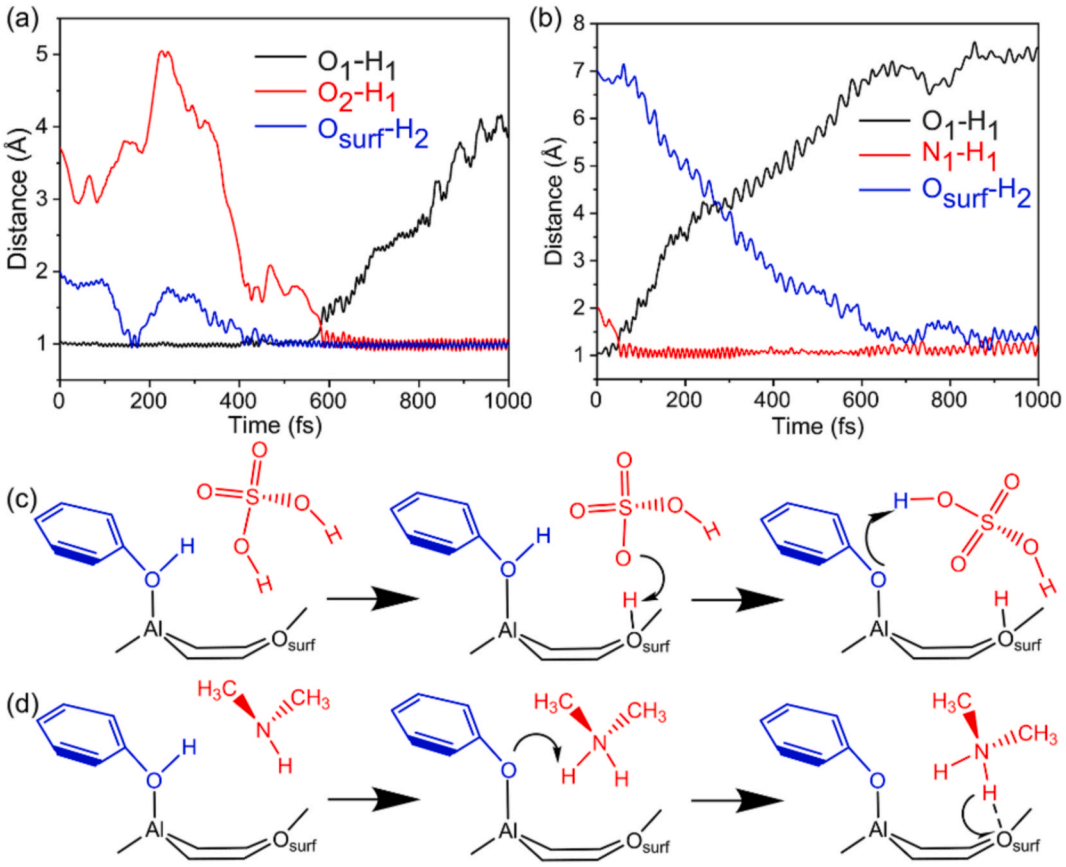

Fig. 7. Key distances change (a) and reaction mechanism (c) for the formation of EPFRs with the participation of SA. (b) and (d) are the key distances change and reaction mechanism, respectively, in the presence of DMA.

Note that this simulation was performed on a clean Al_2O_3 (0001) surface. Firstly, metal oxides in the atmosphere are most likely emitted from combustion sources that are already coated with other organic pollutants and water (Han et al., 2019). Secondly, these coatings form a viscous matrix, which limits the diffusion of acidic and basic pollutants to the metal oxide surface (Liu et al., 2018). Under real atmospheric conditions, these two scenarios and other processes will temper the extent to which the pollutants discussed above influence the reaction mechanism of EPFRs formation.

4. Conclusions

In this study, the influence of different acidic and basic pollutants on EPFRs formation was investigated by using combined DFT and AIMD methods. Specifically, the reaction of phenol, which was used as the aromatic precursor, on an Al_2O_3(0001) surface was employed to model the formation of phenoxy EPFRs. Results indicate that without these acidic and basic pollutants, the reaction is exothermic with an energy barrier of 8.8 kcal mol^{-1}. The presence of these acidic and basic pollutants, which possess the ability to transfer hydrogen atoms, could enhance the formation of EPFRs barrierlessly by promoting the dissociation of phenol by acting as “semi-bridge” or “bridge” roles. However, the corresponding formations are different because of the differing ability to transfer hydrogen atoms. Acidic pollutants are hydrogen atom donors, thus weakening the ability of phenoxy to obtain electrons. Acidic pollutants enhance the formation of EPFRs by first transferring hydrogen atoms to the surface and then combining themselves with aromatic precursors. In contrast, basic pollutants, which are hydrogen atom acceptors, enhance the ability of phenoxy to obtain electrons. Basic pollutants promote the formation of EPFRs by first abstracting hydrogen atoms from aromatic precursors to form phenoxy EPFRs, and then interacting with the surface. Considering the high concentrations of acidic and basic pollutants in local polluted areas, the concentrations of EPFRs may increase significantly due to pollutants’ catalytic effect. These new findings can provide ideas for synergistic control of different kinds of pollutants for improving air quality.

Credit author statement

Li Wang: Data curation, Formal analysis, Investigation, Writing – original draft; Writing – review & editing; Danli Liang: Methodology, Data curation, Writing – review & editing; Jiarong Liu: Writing - Reviewing and Editing, Validation, Visualization; Lin Du: Conceptualization, Writing - Reviewing and Editing; Eric Vejerano: Writing - Reviewing and Editing, Validation; Xiuhui Zhang: Conceptualization, Writing – review & editing, Formal analysis, Supervision.

Declaration of competing interest

The authors declare that they have no known competing financial interests or personal relationships that could have appeared to influence the work reported in this paper.

Acknowledgments

This work was supported by the National Natural Science Foundation of China (Nos. 21976015). Eric Vejerano was supported by the United States National Science Foundation through grants 1738337 and 1834638.

Appendix A. Supplementary data

Supplementary data to this article can be found online at https://doi.org/10.1016/j.chemosphere.2022.134854.

References

Ahmed, O.H., Altarawneh, M., Al-Harahsheh, M., Jiang, Z.T., Dlugogorski, B.Z., 2020. Formation of phenoxy-type environmental persistent free radicals (EPFRs) from dissociative adsorption of phenol on Cu/Fe and their partial oxides. Chemosphere 240, 124921–124932.

Balakrishna, S., Lomnicki, S., McAvey, K.M., Cole, R.B., Dellinger, B., Cormier, S.A., 2009. Environmentally persistent free radicals amplify ultrafine particle mediated cellular oxidative stress and cytotoxicity. Part. Fibre Toxicol. 6, 14.

Beck, A.D., 1993. Density-functional thermochemistry. III. The role of exact exchange. J. Chem. Phys. 98, 5648–5653.

Blöchl, P.E., 1994. Projector augmented-wave method. Phys. Rev. B 50, 17953.

Bouo, F.X., Kouame, J.K., Tchetche, Y., Kre, R.N., Mousse, M.L., Assamoi, P., Cautenet, S., Cautenet, G., 2011. Redistribution of free tropospheric chemical species over west africa: radicals (OH and HO_2, peroxide (H_2O_2) and acids (HNO_3 and H_2SO_4). Chemosphere 84, 1617–1629.

Chang, Y., Zou, Z., Zhang, Y., Deng, C., Hu, J., Shi, Z., Dore, A.J., Collett Jr., J.L., 2019. Assessing contributions of agricultural and nonagricultural emissions to atmospheric ammonia in a Chinese megacity. Environ. Sci. Technol. 53, 1822–1833.

Chen, Q.C., Sun, H.Y., Mu, Z., Wang, Y.Q., Li, Y.G., Zhang, L.X., Wang, M.M., Zhang, Z. M., 2019. Characteristics of environmentally persistent free radicals in $PM_{2.5}$: concentrations, species and sources in Xi'an, northwestern China. Environ. Pollut. 247, 18–26.

Chen, Y., Guo, H., Nah, T., Tanner, D.J., Sullivan, A.P., Takeuchi, M., Gao, Z., Vasilakos, P., Russell, A.G., Baumann, K., Huey, L.G., Weber, R.J., Ng, N.L., 2021. Low-molecular-weight carboxylic acids in the southeastern U.S.: formation, partitioning, and implications for organic aerosol aging. Environ. Sci. Technol. 55, 6688–6699.

Cheng, P., Zhao, X., El-Ramady, H., Elsakhawy, T., Waigi, M.G., Ling, W., 2022. Formation of environmentally persistent free radicals from photodegradation of triclosan by metal oxides/silica suspensions and particles. Chemosphere 290, 133322.

Dai, L., Wang, H., Zhou, L., An, J., Tang, L., Lu, C., Yan, W., Liu, R., Kong, S., Chen, M., Lee, S., Yu, H., 2017. Regional and local new particle formation events observed in the Yangtze river delta region, China. J. Geophys. Res. Atmos. 122, 2389–2402.

Dellinger, B., Loninicki, S., Khachatryan, L., Maskos, Z., Hall, R.W., Adounkpe, J., McFerrin, C., Truong, H., 2007. Formation and stabilization of persistent free radicals. Proc. Combust. Inst. 31, 521–528.

Feng, W., Zhang, Y., Huang, L., Li, Y., Guo, Q., Peng, H., Shi, L., 2022. Spatial distribution, pollution characterization, and risk assessment of environmentally persistent free radicals in urban road dust from central China. Environ. Pollut. 298, 118861.

Ge, X., Wexler, A.S., Clegg, S.L., 2011. Atmospheric amines – part I. A review. Atmos. Environ. 45, 524–546.

Gehling, W., Khachatryan, L., Dellinger, B., 2014. Hydroxyl radical generation from environmentally persistent free radicals (EPFRs) in $PM_{2.5}$. Environ. Sci. Technol. 48, 4266–4272.

Guo, C., Richmond-Bryant, J., 2021. A critical review of environmentally persistent free radical (EPFR) solvent extraction methodology and retrieval efficiency. Chemosphere 284, 131353.

Han, Y., Gong, Z., Ye, J., Liu, P., McKinney, K.A., Martin, S.T., 2019. Quantifying the role of the relative humidity-dependent physical state of organic particulate matter in the uptake of semivolatile organic molecules. Environ. Sci. Technol. 53, 13209–13218.

He, G., Ma, J., He, H., 2018. Role of carbonaceous aerosols in catalyzing sulfate formation. ACS Catal. 8, 3825–3832.

Henkelman, G., Arnaldsson, A., Jónsson, H., 2006. A fast and robust algorithm for bader decomposition of charge density. Comput. Mater. Sci. 36, 354–360.

Henkelman, G., Uberuaga, B.P., Jónsson, H., 2000. A climbing image nudged elastic band method for finding saddle points and minimum energy paths. J. Chem. Phys. 113, 9901–9904.

Jayan, R., Islam, M.M., 2021. Single-atom catalysts for improved cathode performance in Na–S batteries: a density functional theory (DFT) study. J. Phys. Chem. C 125, 4458–4467.

Jia, R., Fan, M., Shao, S., Yu, Y., 2021. Urbanization and haze-governance performance: evidence from China's 248 cities. J. Environ. Manag. 288, 112436.

Julin, J., Murphy, B.N., Patoulias, D., Fountoukis, C., Olenius, T., Pandis, S.N., Riipinen, I., 2018. Impacts of future european emission reductions on aerosol particle number concentrations accounting for effects of ammonia, amines, and organic species. Environ. Sci. Technol. 52, 692–700.

Khachatryan, L., Vejerano, E., Lomnicki, S., Dellinger, B., 2011. Environmentally persistent free radicals (EPFRs). 1. Generation of reactive oxygen species in aqueous solutions. Environ. Sci. Technol. 45, 8559–8566.

Kiruri, L.W., Khachatryan, L., Dellinger, B., Lomnicki, S., 2014. Effect of copper oxide concentration on the formation and persistency of environmentally persistent free radicals (EPFRs) in particulates. Environ. Sci. Technol. 48, 2212–2217.

Laughner, J.L., Cohen, R.C., 2019. Direct observation of changing NO_x lifetime in north American cities. Science 366, 723–727.

Li, G., Han, J., Wang, H., Zhu, X., Ge, Q., 2015. Role of dissociation of phenol in its selective hydrogenation on Pt(111) and Pd(111). ACS Catal. 5, 2009–2016.

Li, H., Pan, B., Liao, S.H., Zhang, D., Xing, B.S., 2014. Formation of environmentally persistent free radicals as the mechanism for reduced catechol degradation on hematite-silica surface under UV irradiation. Environ. Pollut. 188, 153–158.

Li, X., Li, Y., Lawler, M.J., Hao, J., Smith, J.N., Jiang, J., 2021. Composition of ultrafine particles in urban Beijing: measurement using a thermal desorption chemical ionization mass spectrometer. Environ. Sci. Technol. 55, 2859–2868.

Li, Z., Guo, S., Li, Z., Wang, Y., Hu, Y., Xing, Y., Liu, G., Fang, R., Zhu, H., 2020. $PM_{2.5}$ associated phenols, phthalates, and water soluble ions from five stationary combustion sources. Aerosol Air Qual. Res. 20, 61–71.

Lian, H.Y., Pang, S.F., He, X., Yang, M., Ma, J.B., Zhang, Y.H., 2020. Heterogeneous reactions of isoprene and oozone on alpha-Al_2O_3: the suppression effect of relative humidity. Chemosphere 240, 124744.

Liu, L., Zhong, J., Vehkamaki, H., Kurten, T., Du, L., Zhang, X., Francisco, J.S., Zeng, X. C., 2019. Unexpected quenching effect on new particle formation from the atmospheric reaction of methanol with SO_3. Proc. Natl. Acad. Sci. U.S.A. 116, 24966–24971.

Liu, P., Li, Y.J., Wang, Y., Bateman, A.P., Zhang, Y., Gong, Z., Bertram, A.K., Martin, S.T., 2018. Highly viscous states affect the browning of atmospheric organic particulate matter. ACS Cent. Sci. 4, 207–215.

Liu, S., Pedersen, L.G., 2009. Estimation of molecular acidity via electrostatic potential at the nucleus and valence natural atomic orbitals. J. Phys. Chem. 113, 3648–3655.

Łodziana, Z., Nørskov, J.K., 2001. Adsorption of Cu and Pd on α-Al_2O_3(0001) surfaces with different stoichiometries. J. Chem. Phys. 115, 11261–11267.

Lu, T., Manzetti, S., 2014. Wavefunction and reactivity study of benzo [a] pyrene diol epoxide and its enantiomeric forms. Struct. Chem. 25, 1521–1533.

Mao, J., Yu, F., Zhang, Y., An, J., Wang, L., Zheng, J., Yao, L., Luo, G., Ma, W., Yu, Q., Huang, C., Li, L., Chen, L., 2018. High-resolution modeling of gaseous methylamines over a polluted region in China: source-dependent emissions and implications of spatial variations. Atmos. Chem. Phys. 18, 7933–7950.

Messaykeh, M., Goniakowski, J., Cabailh, G., Jupille, J., Lazzari, R., Lagarde, P., Trcera, N., 2019. Chromium adsorption reveals a persistent hydroxylation of vacuum-annealed α-Al_2O_3(0001). J. Phys. Chem. C 123, 29245–29254.

Ning, A., Zhang, H., Zhang, X., Li, Z., Zhang, Y., Xu, Y., Ge, M., 2020. A molecular-scale study on the role of methanesulfinic acid in marine new particle formation. Atmos. Environ. 227.

Pan, B., Li, H., Lang, D., Xing, B.S., 2019a. Environmentally persistent free radicals: occurrence, formation mechanisms and implications. Environ. Pollut. 248, 320–331.

Pan, W.X., Chang, J.M., Liu, X., Xue, Q., Fu, J.J., Zhang, A.Q., 2019b. Interfacial formation of environmentally persistent free aadicals-a theoretical investigation on pentachlorophenol activation on montmorillonite in $PM_{2.5}$. Ecotoxicol. Environ. Saf. 169, 623–630.

Pan, Y., Tian, S., Liu, D., Fang, Y., Zhu, X., Zhang, Q., Zheng, B., Michalski, G., Wang, Y., 2016. Fossil fuel combustion-related emissions dominate atmospheric ammonia sources during severe haze episodes: evidence from (15)N-stable isotope in size-resolved aerosol ammonium. Environ. Sci. Technol. 50, 8049–8056.

Patterson, M.C., Keilbart, N.D., Kiruri, L.W., Thibodeaux, C.A., Lomnicki, S., Kurtz, R.L., Poliakoff, E.D., Dellinger, B., Sprunger, P.T., 2013. EPFR formation from phenol adsorption on Al_2O_3 and TiO_2: EPR and EELS studies. Chem. Phys. 422, 277–282.

Perdew, J.P., Burke, K., Ernzerhof, M., 1996. Generalized gradient approximation made simple. Phys. Rev. Lett. 77, 3865.

Qian, R., Zhang, S., Peng, C., Zhang, L., Yang, F., Tian, M., Huang, R., Wang, Q., Chen, Q., Yao, X., Chen, Y., 2020. Characteristics and potential exposure risks of environmentally persistent free radicals in $PM_{2.5}$ in the three gorges reservoir area, southwestern China. Chemosphere 252, 126425–126434.

Qin, L., Yang, L., Liu, X., Li, C., Lin, B., Zheng, M., Liu, G., 2021. Formation of environmentally persistent free radicals from thermochemical reactions of catechol. Sci. Total Environ. 772, 145313.

Saravia, J., Lee, G.I., Lomnicki, S., Dellinger, B., Cormier, S.A., 2013. Particulate matter containing environmentally persistent free radicals and adverse infant respiratory health effects: a review. J. Biochem. Mol. Toxicol. 27, 56–68.

Savin, A., Nesper, R., Wengert, S., Fässler, T.F., 1997. ELF: the electron localization function. Angew. Chem., Int. Ed. Engl. 36, 1808–1832.

Sun, J., Liang, M., Shi, Z., Shen, F., Li, J., Huang, L., Ge, X., Chen, Q., Sun, Y., Zhang, Y., Chang, Y., Ji, D., Ying, Q., Zhang, H., Kota, S.H., Hu, J., 2019. Investigating the $PM_{2.5}$ mass concentration growth processes during 2013-2016 in Beijing and Shanghai. Chemosphere 221, 452–463.

Truong, H., Lomnicki, S., Dellinger, B., 2010. Potential for misidentification of environmentally persistent free radicals as molecular pollutants in particulate matter. Environ. Sci. Technol. 44, 1933–1939.

Tsai, Y.I., Kuo, S.-C., 2013. Contributions of low molecular weight carboxylic acids to aerosols and wet deposition in a natural subtropical broad-leaved forest environment. Atmos. Environ. 81, 270–279.

VandeVondele, J., Krack, M., Mohamed, F., Parrinello, M., Chassaing, T., Hutter, J., 2005. Quickstep: fast and accurate density functional calculations using a mixed Gaussian and plane waves approach. Comput. Phys. Commun. 167, 103–128.

Vejerano, E., Lomnicki, S., Dellinger, B., 2012a. Lifetime of combustion-generated environmentally persistent free radicals on Zn(II)O and other transition metal oxides. J. Environ. Monit. 14, 2803–2806.

Vejerano, E., Lomnicki, S.M., Dellinger, B., 2012b. Formation and stabilization of combustion-generated, environmentally persistent radicals on Ni(II)O supported on a silica surface. Environ. Sci. Technol. 46, 9406–9411.

Vejerano, E.P., Rao, G., Khachatryan, L., Cormier, S.A., Lomnicki, S., 2018. Environmentally persistent free radicals: insights on a new class of pollutants. Environ. Sci. Technol. 52, 2468–2481.

Wallin, E., Andersson, J.M., Münger, E.P., Chirita, V., Helmersson, U., 2006. Ab initio studies of Al, O, and O_2 adsorption on α−Al_2O_3(0001) surfaces. Phys. Rev. B 74, 125409.

Wang, C., Huang, Y.P., Zhang, Z.T., Cai, Z.W., 2020a. Levels, spatial distribution, and source identification of airborne environmentally persistent free radicals from tree leaves. Environ. Pollut. 257, 113353–113362.

Wang, M., Kong, W., Marten, R., He, X.C., Chen, D., Pfeifer, J., Heitto, A., Kontkanen, J., Dada, L., Kurten, A., Yli-Juuti, T., Manninen, H.E., Amanatidis, S., Amorim, A., Baalbaki, R., Baccarini, A., Bell, D.M., Bertozzi, B., Brakling, S., Brilke, S., Murillo, L. C., Chiu, R., Chu, B., De Menezes, L.P., Duplissy, J., Finkenzeller, H., Carracedo, L.G., Granzin, M., Guida, R., Hansel, A., Hofbauer, V., Krechmer, J., Lehtipalo, K., Lamkaddam, H., Lampimaki, M., Lee, C.P., Makhmutov, V., Marie, G., Mathot, S., Mauldin, R.L., Mentler, B., Muller, T., Onnela, A., Partoll, E., Petaja, T., Philippov, M., Pospisilova, V., Ranjithkumar, A., Rissanen, M., Rorup, B., Scholz, W., Shen, J., Simon, M., Sipila, M., Steiner, G., Stolzenburg, D., Tham, Y.J., Tome, A., Wagner, A.C., Wang, D.S., Wang, Y., Weber, S.K., Winkler, P.M., Wlasits, P.J., Wu, Y., Xiao, M., Ye, Q., Zauner-Wieczorek, M., Zhou, X., Volkamer, R., Riipinen, I., Dommen, J., Curtius, J., Baltensperger, U., Kulmala, M., Worsnop, D.R., Kirkby, J., Seinfeld, J.H., El-Haddad, I., Flagan, R.C., Donahue, N.M., 2020b. Rapid growth of new atmospheric particles by nitric acid and ammonia condensation. Nature 581, 184–189.

Wang, Y.Q., Li, S.P., Wang, M.M., Sun, H.Y., Mu, Z., Zhang, L.X., Li, Y.G., Chen, Q.C., 2019. Source apportionment of environmentally persistent free radicals (EPFRs) in $PM_{2.5}$ over Xi'an, China. Sci. Total Environ. 689, 193–202.

Wu, J.Z., Liu, Y., Zhang, J., Zhou, J.Z., Liu, Z.X., Zhang, X., Qian, G.R., 2020. A density functional theory calculation for revealing environmentally persistent free radicals generated on PbO particulate. Chemosphere 255, 126910–126916.

Xu, J., Finlayson-Pitts, B.J., Gerber, R.B., 2017. Proton transfer in mixed clusters of methanesulfonic acid, methylamine, and oxalic acid: implications for atmospheric particle formation. J. Phys. Chem. 121, 2377–2385.

Xu, M., Wu, T., Tang, Y.-T., Chen, T., Khachatryan, L., Iyer, P.R., Guo, D., Chen, A., Lyu, M., Li, J., Liu, J., Li, D., Zuo, Y., Zhang, S., Wang, Y., Meng, Y., Qi, F., 2019. Environmentally persistent free radicals in $PM_{2.5}$: a review. Waste Disposal Sustain. Energy 1, 177–197.

Yang, L., Nie, W., Liu, Y., Xu, Z., Xiao, M., Qi, X., Li, Y., Wang, R., Zou, J., Paasonen, P., Yan, C., Xu, Z., Wang, J., Zhou, C., Yuan, J., Sun, J., Chi, X., Kerminen, V.-M., Kulmala, M., Ding, A., 2021. Toward building a physical proxy for gas-phase sulfuric acid concentration based on its budget analysis in polluted Yangtze river delta, east China. Environ. Sci. Technol. 55, 6665–6676.

Zhang, F., Wang, Y., Peng, J., Chen, L., Sun, Y., Duan, L., Ge, X., Li, Y., Zhao, J., Liu, C., 2020a. An unexpected catalyst dominates formation and radiative forcing of regional haze. Proc. Natl. Acad. Sci. U.S.A. 117, 3960–3966.

Zhang, R., Wang, G., Guo, S., Zamora, M.L., Ying, Q., Lin, Y., Wang, W., Hu, M., Wang, Y., 2015. Formation of urban fine particulate matter. Chem. Rev. 115, 3803–3855.

Zhang, X., Gu, W., Ma, Z., Liu, Y., Ru, H., Zhou, J., Zang, Y., Xu, Z., Qian, G., 2020b. Short-term exposure to ZnO/MCB persistent free radical particles causes mouse lung lesions via inflammatory reactions and apoptosis pathways. Environ. Pollut. 261, 114039.

Zhao, Y., Chen, X., Shen, J., Xu, A., Wang, Y., Meng, Q., Xu, P., 2021a. Black tea alleviates particulate matter-induced lung injury via the gut-lung axis in mice. J. Agric. Food Chem. 69, 15362–15373.

Zhao, Z., Wu, M., Zhou, D., Chen, Q., Li, H., Lang, D., Pan, B., Xing, B., 2021b. CuO and TiO_2 particles generated more stable and stronger epfrs in dark than under UV-irradiation. Sci. Total Environ. 775, 145555–145564.